Progress In Electromagnetics Research, PIER 85, 303–322, 2008

MODAL-EXPANSION ANALYSIS OF A MONOPOLE IN VIBRATING REVERBERATION CHAMBER

H. P. Zhao and Z. X. Shen

School of Electrical and Electronic Engineering
Nanyang Technological University
50 Nanyang Avenue, Singapore 639798, Singapore

Abstract—A modal-expansion method is proposed for the analysis of a monopole antenna in a vibrating reverberation chamber. Inside the chamber, electromagnetic fields are expanded using modal functions. Mode matching process is applied to enforce the boundary conditions at regional interfaces. Boundary conditions on the four side walls of the chamber are imposed by the point matching method. Combining these two matching processes, a set of matrix equations are obtained and the expansion coefficients can then be determined accordingly. The loss from the chamber walls is accounted for through homogeneous material filling. The input impedance and scattering parameter of a monopole in a reverberation chamber are computed and statistical analysis of the scattering parameter is conducted when one of its walls is vibrating.

1. INTRODUCTION

Electromagnetic reverberation enclosures [1] are preferred tools for electromagnetic shielding and interference testing [2]. An interesting and meaningful topic on reverberation chamber (RC) is to extend its application potentials. Compared with the anechoic chamber (AC), RC requires lower cost and smaller size. Therefore, antenna measurement in RC attracts much interest recently. It has been shown that RC can be an alternative to AC for measuring radiation efficiency of small antennas and radiated power of mobile terminals [3]. Measurement of an antenna's free-space input impedance was conducted by Kildal et al. [4] in RC. Moreover, the Rayleigh distributed fading environment in RC can be used for measurement of multiple-input multiple-output (MIMO) antennas [5, 6], which extends its potential beyond what is possible in AC.

In RC, statistical electromagnetic environment is created through changing the boundary conditions continuously. Variation of boundary condition is generally implemented using a rotating stirrer. Although a rotating stirrer works well, it is still meaningful to study new approaches of stirring to simplify the design of RC. Moreover, measurement of small antennas may not need a large working volume. Therefore, alternative methods of stirring have been proposed, such as, electronic stirring [7–9], position stirring [8], vibrating intrinsic reverberation chamber (VIRC) [10] and vibrating reverberation chamber (VRC) [11, 12]. The VRC is a metallic cavity with one of its walls vibrating. The boundary conditions change continuously as the vibrating wall vibrates. To investigate the effectiveness of this newly proposed stirring approach, it is very important to have an analysis tool. With a two-dimensional model, the analysis of VRC was conducted using the geometrical optics method in [11]. Kouveliotis et al. [12] extended that work to three-dimensional structures, but they simply assumed a transmitted wave instead of using a practical antenna as the excitation. In [9], the modal-expansion method was used to investigate the effectiveness of source stirring. However, the authors didn't take the effect of the transmitting antenna into consideration. Most previous work provided analysis of these new types of RC, but little attention was paid to the problem of antennas in RC. In the past three years, Kildal et al. [8, 13] analyzed a dipole in RC using the cavity Green's function, which ingeniously avoided the discretization of the chamber walls, but the computation of cavity Green's function is complex. Furthermore, the position stirring adopted by Kildal is not very practical, because it is difficult to implement in reality. In [14], Nie et al. modeled a monopole in shielded enclosures using the method of moment, but the discretization of enclosure walls leads to a large system of equations.

The modal-expansion method, shown to be efficient and accurate, is widely used in analysis of antennas [15–18] and waveguide [19, 20]. Based on modal-expansion method, this paper introduces a realistic and rigorous analysis of a monopole in vibrating reverberation chamber. The whole structure is divided into three regions and electromagnetic fields in each region are expanded using modal functions derived from Helmholtz equation. Across the interfaces of these regions, mode matching process is applied to enforce the boundary conditions. Then, the point matching method is used to impose boundary conditions on the cavity walls. Combining these two matching processes, we can derive a set of matrix equations with regard to the unknown field expansion coefficients. Once they are solved, input impedance and scattering parameter of the monopole

can then be computed. In the above procedure, the monopole and the cavity walls are treated as perfect electric conductor (PEC). To account for the metallic loss, the homogenous loss model by Kildal [8] is adopted here. To the authors' best knowledge, although the modal-expansion method has been applied to the analysis of a reverberation chamber, most of the previous work simply assumed an empty chamber and ignored the transmitting antenna. This paper aims to provide a rigorous analysis of a monopole in the vibrating reverberation chamber.

The rest of this paper is organized as follows. In Section 2, formulations of field expansion, matching processes and the loss model are presented. Section 3 presents the verification of the proposed method and statistical analysis of the S-parameter at the monopole feed.

2. FORMULATION

2.1. Field Expansions

The general arrangement of a vibrating reverberation chamber (VRC) is depicted in Fig. 1. A monopole, excited through a coaxial waveguide, is fixed on the bottom wall of a metallic chamber. The right side wall, called the vibrating wall, vibrates to change the boundary condition and hence the field distribution inside the chamber. In this paper,

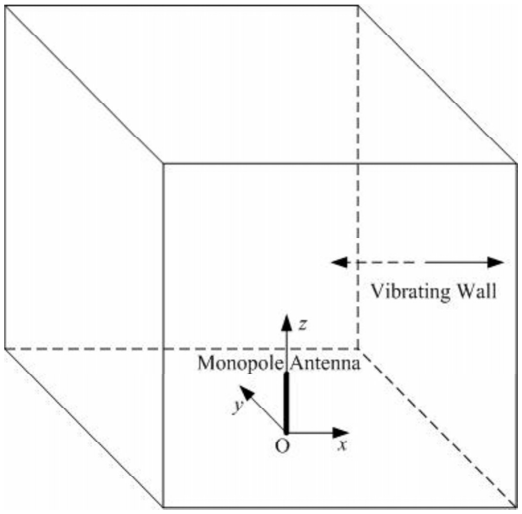

Figure 1. Demonstration of a monopole antenna in a vibrating reverberation chamber.

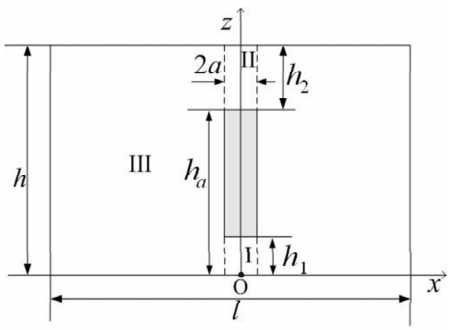

(a) View from the front

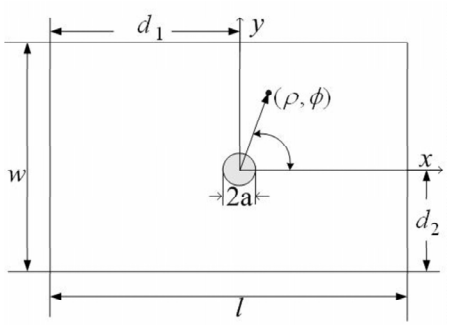

(b) View from the top

Figure 2. Analysis model of a vibrating reverberation chamber excited by a monopole antenna.

excitation of the monopole is represented using the delta gap source model, whose equivalence to the coaxial waveguide excitation has been demonstrated in [21]. The analysis model of this VRC is shown in Fig. 2, where the whole structure of interest is divided into three regions: I, II and III. To obtain the field expansions in each region, we start from the Hertzian electric vector potential function $\vec{F}^e$, which satisfies the following Helmholtz equation:

$$\nabla^2 \vec{F}^e + \omega^2 \mu \epsilon \vec{F}^e = 0 \tag{1}$$

Using the method of separation of variables, we can obtain the expression of $\vec{F}^e$. The magnetic vector potential function $\vec{F}^h$ also satisfies the same Helmholtz equation and can be solved similarly. The

expressions of these two vector potential functions are of the form:

$$\vec{F}^e = \sum_{n=0}^{N}\sum_{m=-M}^{M}\left[a_{mn}^e J_m(k_n\rho) + b_{mn}^e Y_m(k_n\rho)\right]\cos\frac{n\pi z}{d}e^{jm\phi}\vec{i}_z \quad (2a)$$

$$\vec{F}^h = \sum_{n=0}^{N}\sum_{m=-M}^{M}\left[a_{mn}^h J_m(k_n\rho) + b_{mn}^h Y_m(k_n\rho)\right]\sin\frac{n\pi z}{d}e^{jm\phi}\vec{i}_z \quad (2b)$$

where $k_n = \sqrt{k_0^2 - (n\pi/d)^2}$, $k_0^2 = \omega^2\mu\epsilon$ and d is the height of the corresponding region. J_m and Y_m are the m^{th} order first and second kinds Bessel functions, respectively. In regions I and II, which contain the axis $\rho = 0$, the expansion coefficients of Y_m should be zero. Moreover, it is reasonable to assume axial symmetry in regions I and II since the radius of the monopole is rather small. From the vector potential functions, field expansions can be obtained using the relationships between them, which can be found in [22] and are hence omitted here.

For the excitation gap region I, the gap height is rather small, so variation along the z-direction can be ignored and only field components E_z^I and H_ϕ^I are non-zero, which are

$$E_z^I = \frac{A^I}{j\omega\epsilon_0}\frac{J_0(k_0\rho)}{J_0(k_0 a)} \quad (3a)$$

$$H_\phi^I = \frac{A^I}{k_0}\frac{J_0'(k_0\rho)}{J_0(k_0 a)} \quad (3b)$$

For region II between the top end of the monopole and the top wall, we have

$$E_z^{II} = -\frac{1}{j\omega\epsilon_0}\sum_{n=0}^{N_{II}}\frac{k_n^{II}\epsilon_n a_n^{IIe}}{h_2}\frac{J_0(k_n^{II}\rho)}{J_0'(k_n^{II}a)}\cos\frac{n\pi(z-h_a)}{h_2} \quad (4a)$$

$$E_\phi^{II} = j\omega\mu_0\sum_{n=1}^{N_{II}}\frac{\epsilon_n a_n^{IIh}}{k_n^{II}h_2}\frac{J_0'(k_n^{II}\rho)}{J_0(k_n^{II}a)}\sin\frac{n\pi(z-h_a)}{h_2} \quad (4b)$$

$$E_\rho^{II} = \frac{1}{j\omega\epsilon_0}\sum_{n=1}^{N_{II}}\frac{n\pi\epsilon_n a_n^{IIe}}{(h_2)^2}\frac{J_0'(k_n^{II}\rho)}{J_0'(k_n^{II}a)}\sin\frac{n\pi(z-h_a)}{h_2} \quad (4c)$$

$$H_z^{II} = \sum_{n=1}^{N_{II}}\frac{\epsilon_n a_n^{IIh}}{h_2}\frac{J_0(k_n^{II}\rho)}{J_0(k_n^{II}a)}\sin\frac{n\pi(z-h_a)}{h_2} \quad (4d)$$

$$H_\phi^{II} = \sum_{n=0}^{N_{II}} \frac{\epsilon_n a_n^{IIe}}{h_2} \frac{J_0'(k_n^{II}\rho)}{J_0'(k_n^{II}a)} \cos\frac{n\pi(z-h_a)}{h_2} \tag{4e}$$

$$H_\rho^{II} = \sum_{n=1}^{N_{II}} \frac{n\pi\epsilon_n a_n^{IIh}}{k_n^{II}(h_2)^2} \frac{J_0'(k_n^{II}\rho)}{J_0(k_n^{II}a)} \cos\frac{n\pi(z-h_a)}{h_2} \tag{4f}$$

where $\epsilon_n = \begin{bmatrix} 1, & \text{for } n=0 \\ 2, & \text{for } n>0 \end{bmatrix}$.

For region III, similar to [18], normalization is applied to the modal functions to avoid overflow of function values. The new modal functions are

$$U_{1mn}(\rho) = \frac{J_m(k_n^{III}\rho)Y_m(k_n^{III}a) - Y_m(k_n^{III}\rho)J_m(k_n^{III}a)}{J_m(k_n^{III}a_2)Y_m(k_n^{III}a) - Y_m(k_n^{III}a_2)J_m(k_n^{III}a)}$$

$$U_{2mn}(\rho) = \frac{J_m(k_n^{III}\rho)Y_m(k_n^{III}a_2) - Y_m(k_n^{III}\rho)J_m(k_n^{III}a_2)}{J_m(k_n^{III}a)Y_m(k_n^{III}a_2) - Y_m(k_n^{III}a)J_m(k_n^{III}a_2)}$$

$$U_{3mn}(\rho) = \frac{J_m(k_n^{III}\rho)Y_m'(k_n^{III}a) - Y_m(k_n^{III}\rho)J_m'(k_n^{III}a)}{J_m'(k_n^{III}a_2)Y_m'(k_n^{III}a) - Y_m'(k_n^{III}a_2)J_m'(k_n^{III}a)}$$

$$U_{4mn}(\rho) = \frac{J_m(k_n^{III}\rho)Y_m'(k_n^{III}a_2) - Y_m(k_n^{III}\rho)J_m'(k_n^{III}a_2)}{J_m'(k_n^{III}a)Y_m'(k_n^{III}a_2) - Y_m'(k_n^{III}a)J_m'(k_n^{III}a_2)}$$

where a_2 is a constant chosen to be a little larger than the largest distance from the origin to the cavity walls, J_m' and Y_m' represent the derivatives of the mth order first and second kinds Bessel functions, respectively. With these modal functions, electromagnetic fields in region III are expressed as

$$E_z^{III} = \frac{1}{j\omega\epsilon_0} \sum_{n=0}^{N_{III}} \sum_{m=-M_{III}}^{M_{III}} \frac{\epsilon_n}{h} B_{mn}^e(\rho) \cos\frac{n\pi z}{h} e^{jm\phi} \tag{5a}$$

$$\begin{aligned} E_\phi^{III} = & -\frac{1}{j\omega\epsilon_0\rho} \sum_{n=1}^{N_{III}} \sum_{m=-M_{III}}^{M_{III}} \frac{jmn\pi\epsilon_n}{(k_n^{III}h)^2} B_{mn}^e(\rho) \sin\frac{n\pi z}{h} e^{jm\phi} \\ & + j\omega\mu_0 \sum_{n=1}^{N_{III}} \sum_{m=-M_{III}}^{M_{III}} \frac{\epsilon_n}{h} C_{mn}^h(\rho) \sin\frac{n\pi z}{h} e^{jm\phi} \end{aligned} \tag{5b}$$

$$E_\rho^{III} = -\frac{1}{j\omega\epsilon_0}\sum_{n=1}^{N_{III}}\sum_{m=-M_{III}}^{M_{III}}\frac{n\pi\epsilon_n}{k_n^{III}h^2}C_{mn}^e(\rho)\sin\frac{n\pi z}{h}e^{jm\phi}$$
$$-\frac{j\omega\mu_0}{\rho}\sum_{n=1}^{N_{III}}\sum_{m=-M_{III}}^{M_{III}}\frac{jm\epsilon_n}{hk_n^{III}}B_{mn}^h(\rho)\sin\frac{n\pi z}{h}e^{jm\phi} \quad (5c)$$

$$H_z^{III} = \sum_{n=1}^{N_{III}}\sum_{m=-M_{III}}^{M_{III}}\frac{k_n^{III}\epsilon_n}{h}B_{mn}^h(\rho)\sin\frac{n\pi z}{h}e^{jm\phi} \quad (5d)$$

$$H_\phi^{III} = \frac{1}{\rho}\sum_{n=1}^{N_{III}}\sum_{m=-M_{III}}^{M_{III}}\frac{jmn\pi\epsilon_n}{h^2k_n^{III}}B_{mn}^h(\rho)\cos\frac{n\pi z}{h}e^{jm\phi}$$
$$-\sum_{n=0}^{N_{III}}\sum_{m=-M_{III}}^{M_{III}}\frac{\epsilon_n}{k_n^{III}h}C_{mn}^e(\rho)\cos\frac{n\pi z}{h}e^{jm\phi} \quad (5e)$$

$$H_\rho^{III} = \sum_{n=1}^{N_{III}}\sum_{m=-M_{III}}^{M_{III}}\frac{n\pi\epsilon_n}{h^2}C_{mn}^h(\rho)\cos\frac{n\pi z}{h}e^{jm\phi}$$
$$+\frac{1}{\rho}\sum_{n=0}^{N_{III}}\sum_{m=-M_{III}}^{M_{III}}\frac{jm\epsilon_n}{h(k_n^{III})^2}B_{mn}^e(\rho)\cos\frac{n\pi z}{h}e^{jm\phi} \quad (5f)$$

where

$$B_{mn}^e(\rho) = a_{mn}^{IIIe}U_{1mn}(\rho) + b_{mn}^{IIIe}U_{2mn}(\rho),$$
$$B_{mn}^h(\rho) = a_{mn}^{IIIh}U_{3mn}(\rho) + b_{mn}^{IIIh}U_{4mn}(\rho),$$
$$C_{mn}^e(\rho) = a_{mn}^{IIIe}U'_{1mn}(\rho) + b_{mn}^{IIIe}U'_{2mn}(\rho),$$
$$C_{mn}^h(\rho) = a_{mn}^{IIIh}U'_{3mn}(\rho) + b_{mn}^{IIIh}U'_{4mn}(\rho).$$

2.2. Matching Processes

Imposing continuity boundary conditions across the interface $\rho = a$, i.e.,

$$E_z^{III} = \begin{bmatrix} E_z^I, & z\in[0,h_1] \\ 0, & z\in[h_1,h_a] \\ E_z^{II}, & z\in[h_a,h] \end{bmatrix} \quad (6a)$$

$$E_\phi^{III} = \begin{bmatrix} E_\phi^I, & z\in[0,h_1] \\ 0, & z\in[h_1,h_a] \\ E_\phi^{II}, & z\in[h_a,h] \end{bmatrix} \quad (6b)$$

$$H_z^{III} = H_z^{II}, z \in [h_a, h] \tag{6c}$$
$$H_\phi^{III} = H_\phi^{II}, z \in [h_a, h] \tag{6d}$$

and invoking Galerkin's method, we obtain matrix equations (7)

$$\mathbf{B}_p^{IIIe} = \mathbf{M}_I^c A^I \zeta_p + \mathbf{M}_{II}^c \mathbf{V}^{II} \mathbf{A}^{IIe} \zeta_p \tag{7a}$$
$$\mathbf{Y}_p^e \mathbf{B}_p^{IIIe} + \mathbf{B}_p^{IIIh} = \mathbf{M}_{II}^s \mathbf{V}^{IIh} \mathbf{A}^{IIh} \zeta_p \tag{7b}$$
$$\mathbf{A}^{IIh} \zeta_p = (\mathbf{M}_{II}^s)^T \left(\mathbf{Y}_p^{hh} \mathbf{A}_p^{IIIh} + \mathbf{Z}_p^{hh} \mathbf{B}_p^{IIIh} \right) \tag{7c}$$
$$\mathbf{A}^{IIe} \zeta_p = (\mathbf{M}_{II}^c)^T \begin{pmatrix} \mathbf{Y}_p^{he} \mathbf{A}_p^{IIIh} + \mathbf{Z}_p^{he} \mathbf{B}_p^{IIIh} \\ + \mathbf{Y}_p^{ee} \mathbf{A}_p^{IIIe} + \mathbf{Z}_p^{ee} \mathbf{B}_p^{IIIe} \end{pmatrix} \tag{7d}$$

where $\mathbf{A}^{IIe}$, $\mathbf{A}^{IIh}$, $\mathbf{A}_p^{IIIh}$, $\mathbf{B}_p^{IIIh}$, $\mathbf{A}_p^{IIIe}$and $\mathbf{B}_p^{IIIe}$ are vectors with elements of a_n^{IIe}, a_n^{IIh}, a_{pl}^{IIIh}, b_{pl}^{IIIh}, a_{pl}^{IIIe} and b_{pl}^{IIIe}, respectively, and p is a given value of index for the ϕ-directed modal function. Enforcing boundary conditions that tangential electric field components must vanish along the four side chamber walls, matrix equation (8) is obtained using the point matching method.

$$\mathbf{S}^A \mathbf{A}^{IIIe} + \mathbf{S}^B \mathbf{B}^{IIIe} = 0 \tag{8a}$$
$$\mathbf{S}^{Ae} \mathbf{A}^{IIIe} + \mathbf{S}^{Be} \mathbf{B}^{IIIe} = \mathbf{S}^{Ah} \mathbf{A}^{IIIh} + \mathbf{S}^{Bh} \mathbf{B}^{IIIh} \tag{8b}$$

where $\mathbf{A}^{IIIe}$, $\mathbf{B}^{IIIe}$, $\mathbf{A}^{IIIh}$ and $\mathbf{B}^{IIIh}$ are vectors with elements of a_{mn}^{IIIe}, b_{mn}^{IIIe}, a_{mn}^{IIIh} and b_{mn}^{IIIh}, respectively. Elements of all the matrices appearing in Equations (7) and (8) are elucidated in the Appendix for convenience. It should be noted that the field expansions are orthogonalized using the z-directed modal functions before invoking the point matching process so that the computation is simplified to one-dimension. After some manipulations, we have

$$\begin{aligned} &\left[\mathbf{I} - (\mathbf{M}_{II}^s)^T \left(\mathbf{Z}_0^{hh} - \mathbf{Y}_0^{hh} \mathbf{K}_0^h \right) \mathbf{M}_{II}^s \mathbf{V}^{IIh} \right] \mathbf{A}^{IIh} \\ &= (\mathbf{M}_{II}^s)^T \mathbf{Y}_0^{hh} \mathbf{K}_0^e \left(\mathbf{M}_I^c \mathbf{A}^I + \mathbf{M}_{II}^c \mathbf{V}^{II} \mathbf{A}^{IIe} \right) \end{aligned} \tag{9a}$$
$$\begin{aligned} &\left[\mathbf{I} - (\mathbf{M}_{II}^c)^T \left(\mathbf{Y}_0^{ee} \mathbf{K}_0 + \mathbf{Z}_0^{ee} \right) \mathbf{M}_{II}^c \mathbf{V}^{II} \right] \mathbf{A}^{IIe} \\ &= (\mathbf{M}_{II}^c)^T \left(\mathbf{Y}_0^{ee} \mathbf{K}_0 + \mathbf{Z}_0^{ee} \right) \mathbf{M}_I^c \mathbf{A}^I \end{aligned} \tag{9b}$$

where the subscript 0 means $p = 0$ in (7), $\mathbf{K} = -\left(\mathbf{S}^A\right)^{-1} \mathbf{S}^B$, $\mathbf{K}^e = \left(\mathbf{S}^{Ah}\right)^{-1} \left(\mathbf{S}^{Ae} \mathbf{K} + \mathbf{S}^{Be}\right)$ and $\mathbf{K}^h = -\left(\mathbf{S}^{Ah}\right)^{-1} \mathbf{S}^{Bh}$. $\mathbf{K}_0$, $\mathbf{K}_0^e$ and $\mathbf{K}_0^h$, extracted from $\mathbf{K}$, $\mathbf{K}^e$ and $\mathbf{K}^h$, respectively, represent the

relationships between $\mathbf{A}_p^{IIIe}$, $\mathbf{B}_p^{IIIe}$, $\mathbf{A}_p^{IIIh}$ and $\mathbf{B}_p^{IIIh}$ for $p = 0$. From Equation (9), $\mathbf{A}^{IIe}$ and $\mathbf{A}^{IIh}$ can be solved and then all the other expansion coefficients can be obtained from (7a), (7b), (8a) and (8b). It should be noted that, the matrices in (8) are block-diagonal matrices, whose inversion can be computed very efficiently in a block-by-block manner.

2.3. Loss Model

In the previous derivations, the monopole and chamber walls are taken as perfect electric conductor (PEC). To account for the metallic loss, the homogeneous loss model [8] is adopted here. In this model, a constant finite conductivity σ is introduced in the volume of the chamber and then the complex wavenumber is

$$k = \omega\sqrt{\mu_0(\epsilon_0 - j\sigma/\omega)} \tag{10}$$

where ω is the angular frequency, σ is related to the mode bandwidth $\triangle f_1$ by

$$\triangle f_1 = \sigma/(2\pi\epsilon_0) \tag{11}$$

This loss model can be applied to the proposed modal-expansion method easily by computing the wavenumber using (10). σ can be determined by (11) and $\triangle f_1$ is set to 5 MHz for the model used in [8].

3. VALIDATION AND NUMERICAL RESULTS

The proposed method is firstly validated against a 3-D MoM software [23]. After validation, the code is used to investigate the statistical property of the monopole's S-parameter in this section.

3.1. Validation

The first example is a 14.4 cm × 14.4 cm × 14.4 cm metallic cavity with a 5-cm long monopole placed at the bottom centre of the cavity. Fig. 3 demonstrates the input impedance results of the monopole. The right side wall of the cavity is set to be the vibrating wall. Fig. 4 and Fig. 5 show the input impedance when the vibrating wall moves outwards and inwards by 0.4 cm. The agreement between the proposed method and the software is very good in all cases. In these simulations, $N^{III} = 45$, N^{II} is chosen according to the convergence criteria [18]. $2M^{III} + 1$ equals to the number of points matched across the side walls, which

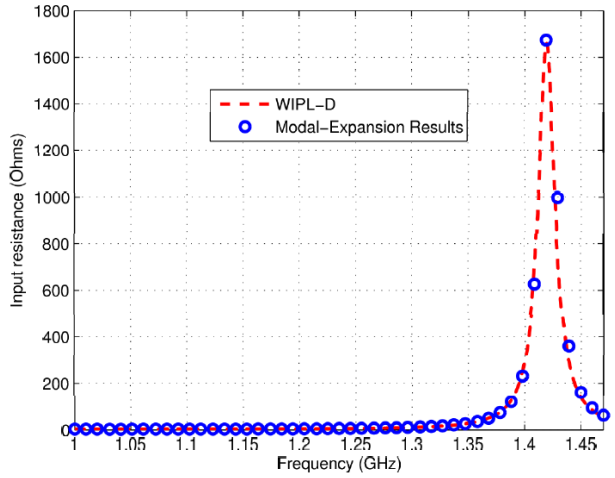

(a) Input resistance

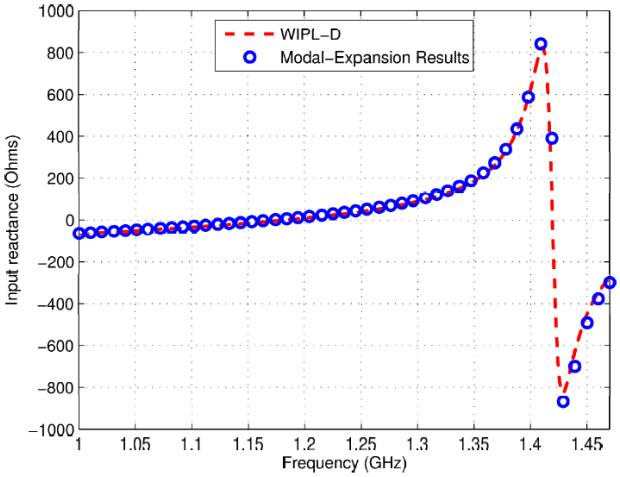

(b) Input reactance

Figure 3. Input impedance of a 5 cm-long monopole placed at the bottom centre of a 14.4 cm × 14.4 cm × 14.4 cm vibrating reverberation chamber. The chamber was loaded with a small homogenous loss represented by a conductivity of $\sigma = 0.001\,\mathrm{S/m}$ through the cavity.

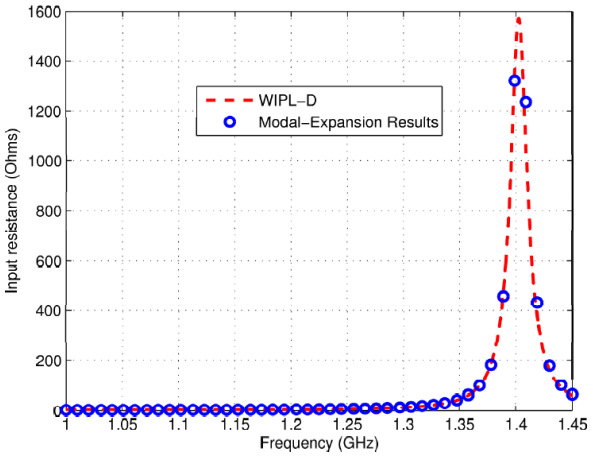

(a) Input resistance

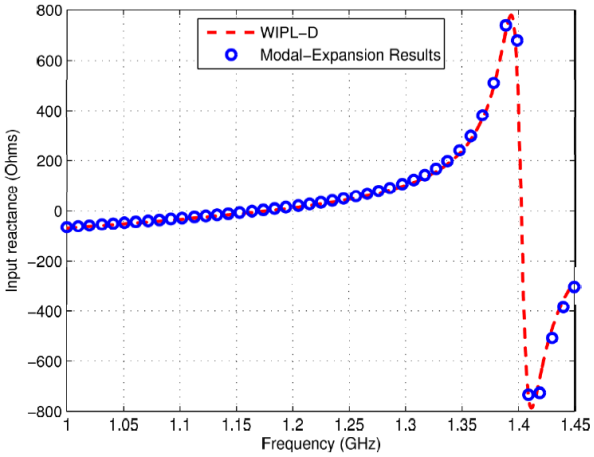

(b) Input reactance

Figure 4. Input impedance of the monopole when the vibrating wall is moved outwards by 0.4 cm.

are sampled following a density of ten points per wavelength [24] across the ϕ direction.

Another example is a rectangular chamber of dimensions 0.779 m $\times$ 1.052 m $\times$ 1.682 m, which are the same as those used in [8]. A 12.5-cm long monopole is placed at the bottom centre of the chamber. The input impedance of the monopole from 0.5 to 0.7 GHz is demonstrated

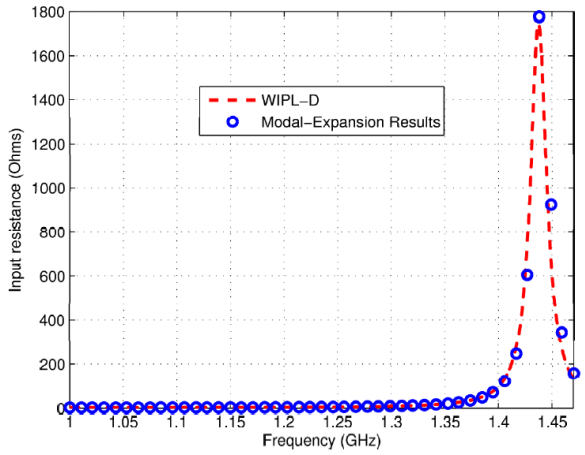

(a) Input resistance

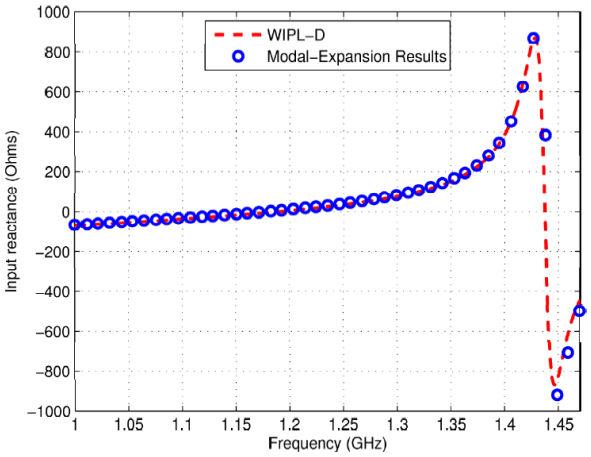

(b) Input reactance

Figure 5. Input impedance of the monopole when the vibrating wall is moved inwards by 0.4 cm.

in Fig. 6–Fig. 8. For this example $N^{III} = 100$ is chosen and the other truncated numbers are determined as described above. The loss of the filling material is determined by (11) to give a bandwidth of 5 MHz, as suggested by [8]. In Fig. 6–Fig. 8, the peak values of resistance correspond to the resonant frequencies where strong coupling between the monopole and the cavity occurs. It is observed that, the effect of

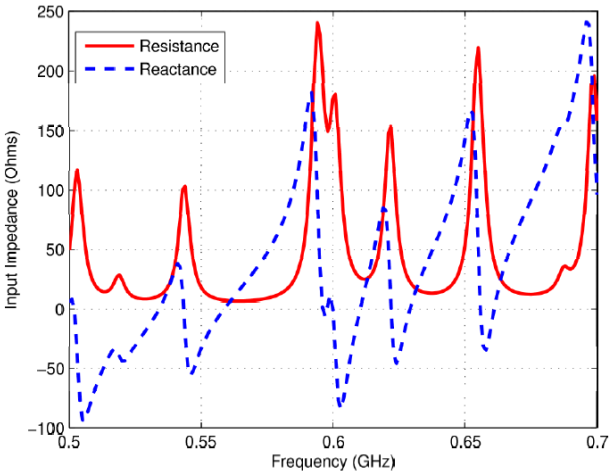

Figure 6. Input impedance of a 12.5 cm-long monopole placed at the bottom centre of a $0.779\,\mathrm{m} \times 1.052\,\mathrm{m} \times 1.682\,\mathrm{m}$ vibrating reverberation chamber. The uniform loss is set to give mode bandwidth of $\triangle f_1 = 5\,\mathrm{MHz}$.

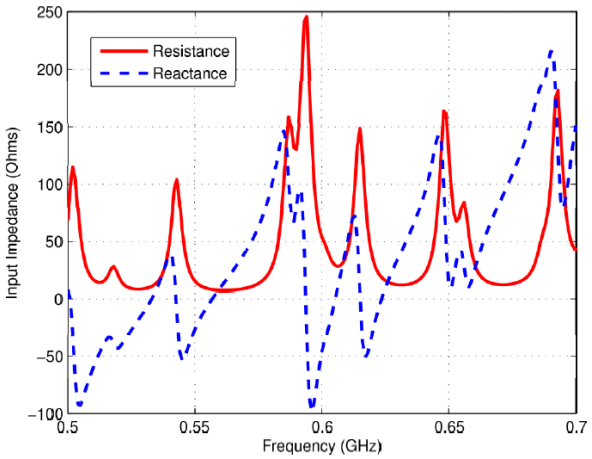

Figure 7. Input impedance of the monopole when the vibrating wall is moved outwards by 1 cm.

the vibrating stirring is more significant at higher frequency. This is reasonable because the electrical size of cavity dimension's variation is larger at higher frequency.

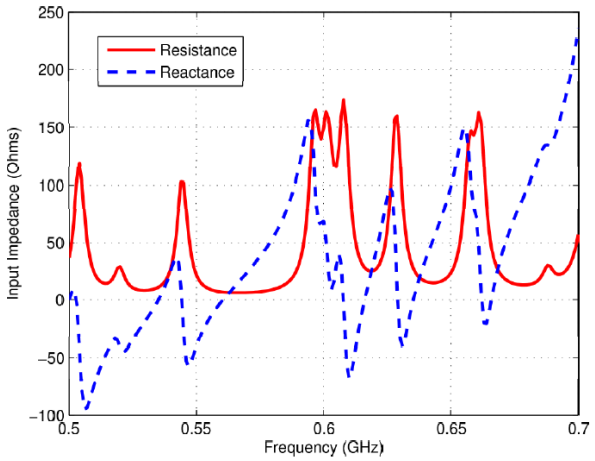

Figure 8. Input impedance of the monopole when the vibrating wall is moved inwards by 1 cm.

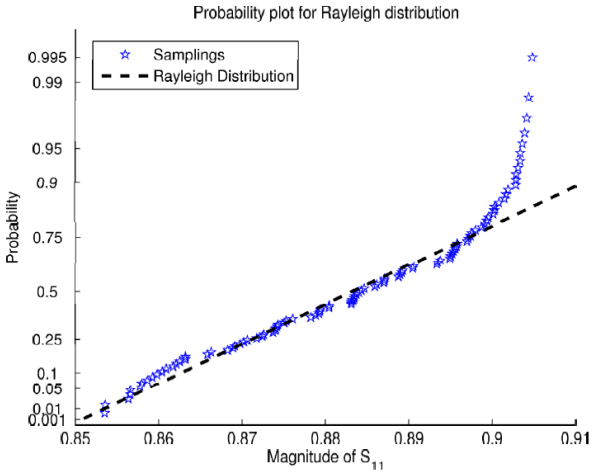

Figure 9. Statistical distribution of $|S_{11}|$ of a 5 cm-long monopole placed at the bottom centre of a 14.4 cm × 14.4 cm × 14.4 cm vibrating reverberation chamber.

3.2. Statistical Analysis of *S*-Parameter

The statistical behavior of the monopole's S-parameter is investigated when the chamber vibrates. The characteristic impedance is 50 Ω because the excitation model is equivalent to a coaxial waveguide.

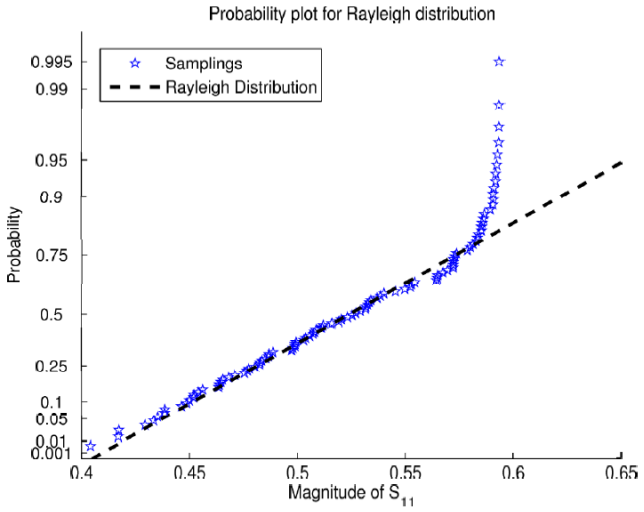

Figure 10. Statistical distribution of S_{11} of a 12.5 cm-long monopole placed at the bottom centre of a 0.779 m $\times$ 1.052 m $\times$ 1.682 m vibrating reverberation chamber.

For the first example, the loss parameter is the same as that used in previous simulations. At the frequency $f = 1.69$ GHz, 100 simulations are conducted. In each simulation, the length of the chamber l is changing and equal to $l_0 + \triangle l$, where l_0 is 14.4 cm and $\triangle l$ is a random variable uniformly distributed in $[-0.4\,\text{cm}, 0.4\text{cm}]$. Fig. 9 gives the statistical distribution of the magnitude of S_{11}. The y-axis values are probabilities from zero to one, though the scale is not linear. The distance between tick marks is the distance between quantiles of the distribution. In the plot, a line is drawn between the first and third quartiles in the data. If the data falls near the line, the samplings obey the Rayleigh distribution well. It is observed that, most of the points are located near to the line. However, marks deviate from the line when the magnitude of S_{11} approaches one. This is because the resistance of the antenna is very small except when strong coupling occurs between the monopole and the cavity, as can be seen from Fig. 3–Fig. 5. If strong coupling doesn't occur, the strong reflection of the cavity walls determines the magnitude of S_{11}, the randomness of which is hence destroyed.

For the second example, 100 simulations are conducted at the frequency $f = 0.6$ GHz and the statistical behaviour of $|S_{11}|$ is demonstrated in Fig. 10. In these 100 simulations, the original length of the chamber l_0 is 0.779 m and the perturbation $\triangle l$ is a random

variable uniformly distributed in $[-0.01\,\mathrm{m}, 0.01\,\mathrm{m}]$. Similarly with the previous case, most marks fall near the straight line except the last a few ones, which correspond to large values of $|S_{11}|$. This is also caused by the strong reflection of the cavity, which destroys the randomness of $|S_{11}|$ at large values.

4. CONCLUSIONS

A modal expansion method has been developed for the rigorous analysis of a monopole in a vibrating reverberation chamber. The loss of the chamber has been taken into account using the homogeneous loss model. The validity of the proposed method have been verified by comparing our results with those obtained from alternative numerical methods. Statistical analysis of the monopole's S-parameters has also been conducted to demonstrate the capability of the method. It is found that the S-parameter doesn't obey the Rayleigh distribution very well under strong reflection. This situation may change if the antenna is properly loaded, as the case in [8].

APPENDIX A. DEFINITION OF MATRICES IN (7)

The elements of matrices occurring in (7) are as follows:

$$M^c_{I(m)} = I^c_{I(m)}, \quad M^c_{II(m,n)} = I^c_{II(m,n)}, \tag{A1a}$$

$$V^{II}_{(m,n)} = -\frac{k^{II}_n \epsilon_n}{h_2} \frac{J_0(k^{II}_n a)}{J'_0(k^{II}_n a)} \zeta_{(m,n)}, \tag{A1b}$$

$$\begin{aligned} I^c_{I(l)} &= \int_0^{h_1} \cos\frac{l\pi z}{h} dz \\ &= \begin{bmatrix} h_1, & \text{for } \ l = 0 \\ \dfrac{h}{l\pi}\left[\sin\left(\dfrac{l\pi h_1}{h}\right)\right], & \text{otherwise} \end{bmatrix}, \end{aligned} \tag{A1c}$$

$$\begin{aligned} I^c_{II(l,n)} &= \int_{h_a}^{h} \cos\frac{l\pi z}{h} \cos\frac{n\pi(z-h_a)}{h_2} dz \\ &= \begin{bmatrix} h_2 & \text{for } \ l = n = 0 \\ -\dfrac{l\pi}{h}\sin\left(\dfrac{l\pi h_a}{h}\right) & \\ \dfrac{}{(l\pi/h)^2 - (n\pi/h_2)^2} & \text{otherwise} \end{bmatrix}. \end{aligned} \tag{A1d}$$

$$M^s_{II(m,n)} = I^s_{II(m,n)}, \tag{A2a}$$

$$I^s_{II(l,n)} = \int_{h_a}^{h} \sin\frac{l\pi z}{h}\sin\frac{n\pi(z-h_a)}{h_2}dz$$
$$= \frac{-\frac{n\pi}{h_2}\sin\left(\frac{l\pi h_a}{h}\right)}{(l\pi/h)^2-(n\pi/h_2)^2} \quad \text{(A2b)}$$
$$Y^e_{p(m,n)} = \frac{1}{k_0^2 a}\frac{jpn\pi}{(k_n^{III})^2 h}\zeta_(m,n), \quad \text{(A2c)}$$
$$V^{IIh}_{(m,n)} = \frac{\epsilon_n}{k_n^{II}h_2}\frac{J_0'(k_n^{II}a)}{J_0(k_n^{II}a)}\zeta_(m,n). \quad \text{(A2d)}$$

$$Y^{hh}_{p(m,n)} = \frac{k_n^{III}\epsilon_n}{h}U_{3pn}(a)\zeta_{(m,n)}, \quad \text{(A3a)}$$
$$Z^{hh}_{p(m,n)} = \frac{k_n^{III}\epsilon_n}{h}U_{4pn}(a)\zeta_{m,n}. \quad \text{(A3b)}$$

$$Y^{he}_{p(m,n)} = \frac{1}{a}\frac{jpn\pi\epsilon_n}{h^2k_n^{III}}U_{3pn}(a)\zeta_{(m,n)}, \quad \text{(A4a)}$$
$$Z^{he}_{p(m,n)} = \frac{1}{a}\frac{jpn\pi\epsilon_n}{h^2k_n^{III}}U_{4pn}(a)\zeta_{(m,n)}, \quad \text{(A4b)}$$
$$Y^{ee}_{p(m,n)} = -\frac{\epsilon_n}{k_n^{III}h}U'_{1pn}(a)\zeta_{(m,n)}, \quad \text{(A4c)}$$
$$Z^{ee}_{p(m,n)} = -\frac{\epsilon_n}{k_n^{III}h}U'_{2pn}(a)\zeta_{(m,n)}. \quad \text{(A4d)}$$

APPENDIX B. DEFINITION OF MATRICES IN (8)

Matrices in (8) are block-diagonal and the lth block is given as follows,

$$S^A_{l(m,n)} = U_{1pl}(\rho_m)e^{jp\phi_m} \quad \text{(B1a)}$$
$$S^B_{l(m,n)} = U_{2pl}(\rho_m)e^{jp\phi_m} \quad \text{(B1b)}$$

where $p = n - M_{III}$.

On the walls $x = 0$ and $x = l$,

$$S^{Ae}_{l(m,n)} = -\frac{1}{k_0^2}\frac{l\pi}{k_l^{III}h}\left[\frac{jp}{k_l^{III}\rho_m}U_{1pl}(\rho_m)+\tan\phi_m U'_{1pl}(\rho_m)\right]e^{jp\phi_m} \quad \text{(B2a)}$$
$$S^{Be}_{l(m,n)} = -\frac{1}{k_0^2}\frac{l\pi}{k_l^{III}h}\left[\frac{jp}{k_l^{III}\rho_m}U_{2pl}(\rho_m)+\tan\phi_m U'_{2pl}(\rho_m)\right]e^{jp\phi_m} \quad \text{(B2b)}$$

$$S^{Ah}_{l(m,n)} = \left[U'_{3pl}(\rho_m) - \frac{jp\tan\phi_m}{k_l^{III}\rho_m}U_{3pl}(\rho_m)\right]e^{jp\phi_m} \quad \text{(B2c)}$$

$$S^{Bh}_{l(m,n)} = \left[U'_{4pl}(\rho_m) - \frac{jp\tan\phi_m}{k_l^{III}\rho_m}U_{4pl}(\rho_m)\right]e^{jp\phi_m} \quad \text{(B2d)}$$

where $p = n - M_{III}$.

On the walls $y = 0$ and $y = w$,

$$S^{Ae}_{l(m,n)} = \frac{1}{k_0^2}\frac{l\pi}{k_l^{III}h}\left[\frac{jp\tan\phi_m}{k_l^{III}\rho_m}U_{1pl}(\rho_m) - U'_{1pl}(\rho_m)\right]e^{jp\phi_m} \quad \text{(B3a)}$$

$$S^{Be}_{l(m,n)} = \frac{1}{k_0^2}\frac{l\pi}{k_l^{III}h}\left[\frac{jp\tan\phi_m}{k_l^{III}\rho_m}U_{2pl}(\rho_m) - U'_{2pl}(\rho_m)\right]e^{jp\phi_m} \quad \text{(B3b)}$$

$$S^{Ah}_{l(m,n)} = -\left[\tan\phi_m U'_{3pl}(\rho_m) + \frac{jp}{k_l^{III}\rho_m}U_{3pl}(\rho_m)\right]e^{jp\phi_m} \quad \text{(B3c)}$$

$$S^{Bh}_{l(m,n)} = -\left[\tan\phi_m U'_{4pl}(\rho_m) + \frac{jp}{k_l^{III}\rho_m}U_{4pl}(\rho_m)\right]e^{jp\phi_m} \quad \text{(B3d)}$$

where $p = n - M_{III}$.

REFERENCES

1. Ma, M., "Understanding reverberating chambers as an alternative facility for EMC testing," *J. of Electromagn. Waves and Appl.*, Vol. 2, No. 3–4, 339–351, 1988.
2. Wang, Y., W. Koh, and C. Lee, "Coupling cross section and shielding effectiveness measurements on a coaxial cable by both mode-tuned reverberation chamber and Gtem cell methodologies," *Progress In Electromagnetics Research*, PIER 47, 61–73, 2004.
3. Serafimov, N., P.-S. Kildal, and T. Bolin, "Comparison between radiation efficiencies of phone antennas and radiated power of mobile phones measured in anechoic chamber and reverberation chamber," *Proc. IEEE Antennas Propag. Soc. Int. Symp.*, Vol. 2, 478–481, Jun. 2002.
4. Kildal, P.-S., C. Carlsson, and J. Yang, "Measurement of free space impedances of small antennas in reverberation chambers," *Microw. Opt. Tech. Lett.*, Vol. 32, No. 2, 112–115, Jan. 2002.
5. Rosengren, K. and P.-S. Kildal, "Radiation efficiency, correlation, diversity gain, and capacity of a six monopole antenna array for a MIMO system: Theory, simulation and measurement

in reverberation chamber," *Proc. IEEE Microw. Antennas and Propag.*, Vol. 152, No. 1, 7–16, 2005.

6. Khaleghi, A., "Diversity techniques with parallel dipole antennas: Radiation pattern analysis," *Progress In Electromagnetics Research*, PIER 64, 23–42, 2006.
7. Hill, D., "Electronic mode stirring for reverberation chambers," *IEEE Trans. Electromagn. Compat.*, Vol. 36, No. 4, 294–299, 1994.
8. Carlberg, U., P.-S. Kildal, and J. Carlsson, "Study of antennas in reverberation chamber using method of moments with cavity Green's function calculated by ewald summation," *IEEE Trans. Electromagn. Compat.*, Vol. 47, No. 4, 805–814, 2005.
9. Cerri, G., V. Primiani, S. Pennesi, and P. Russo, "Source stirring mode for reverberation chambers," *IEEE Trans. Electromagn. Compat.*, Vol. 47, No. 4, 815–823, 2005.
10. Kouveliotis, N., P. Trakadas, and C. Capsalis, "FDTD modelling of a vibrating intrinsic reverberation chamber," *J. of Electromagn. Waves and Appl.*, Vol. 17, No. 6, 849–850, 2003.
11. Cappetta, L., M. Feo, V. Fiumara, V. Pierro, and I. Pinto, "Electromagnetic chaos in mode stirred reverberation enclosures," *IEEE Trans. Electromagn. Compat.*, Vol. 40, No. 3, 185–192, 1998.
12. Kouveliotis, N., P. Trakadas, and C. Capsalis, "Theoretical investigation of the field conditions in a vibrating reverberation chamber with an unstirred component," *IEEE Trans. Electromagn. Compat.*, Vol. 45, No. 1, 77–80, 2003.
13. Karlsson, K., J. Carlsson, and P.-S. Kildal, "Reverberation chamber for antenna measurements: modeling using method of moments, spectral domain techniques, and asymptote extraction," *IEEE Trans. Electromagn. Compat.*, Vol. 54, No. 11, 3106–3113, 2006.
14. Nie, X., N. Yuan, L. Li, and Y. Gan, "Accurate modeling of monopole antennas in shielded enclosures with apertures," *Progress In Electromagnetics Research*, PIER 79, 251–262, 2008.
15. Kim, J. and H. Eom, "Radiation from multiple annular slots on a circular cylindrical cavity," *J. of Electromagn. Waves and Appl.*, Vol. 21, No. 1, 47–56, 2007.
16. Ock, J. and H. Eom, "Radiation of a hertzian dipole in a short-ended conducting circular cylinder with narrow circumferential slots," *Progress In Electromagnetics Research Letters*, Vol. 2, 11–20, 2008.
17. Shen, Z. and R. H. MacPhie, "Theoretical modeling of multi-sleeve monopole antennas," *Progress In Electromagnetics Research*,

PIER 31, 31–54, 2001.

18. Shen, Z. and R. MacPhie, "Rigorous evaluation of the input impedance of a sleeve monopole by modal-expansion method," *IEEE Trans. Antennas Propagat.*, Vol. 44, No. 12, 1584–1591, 1996.
19. Kuwano, S., M. Deno, and K. Kokubun, "A precise mode-matching technique for characterizing an H-plane waveguide Y-junction with an arbitrary angle," *J. of Electromagn. Waves and Appl.*, Vol. 17, No. 7, 969–987, 2003.
20. Jiang, Z., Z. Shen, and X. Shan, "Mode-matching analysis of waveguide T-junction loaded with an H-plane dielectric slab," *J. of Electromagn. Waves and Appl.*, Vol. 16, No. 11, 1613–1614, 2002.
21. Akbarzadeh, A. and Z. Shen, "On the gap source model for monopole antennas," *IEEE Antennas Wireless Propag. Lett.*, Vol. 7, 115–118, 2008.
22. Bladel, J., *Electromagnetic Fields*, John Wiley and Sons, New York, 2007.
23. Kolundzija, B., J. Ognjanovic, and T. Sarkar, *WIPL-D, Electromagnetic Modeling of Composite Metallic and Dielectric Structures*, Artech House, MA, 2000.
24. Huang, E. and A. Fung, "An application of sampling theorem to moment method simulation in surface scattering," *J. of Electromagn. Waves and Appl.*, Vol. 20, No. 4, 531–546, 2006.